doi:10.26443/seismica.v5i1.2015

Atmospheric Signals Recorded by Seismometers in the Sub-Seismic Frequency Band

Piero Poli *[1], **Josipa Majstorović** [2], **T. Dylan Mikesell** [3]

[1]University of Padova, Department of Geoscience, Padova, Italy, [2]Josip Juraj Strossmayer University of Osijek, Department of Physics, Osijek, Croatia, [3]Norwegian Geotechnical Institute, Oslo, Norway

Author contributions: *Formal Analysis*: Piero Poli, Josipa Majstorović, T. Dylan Mikesell. *Writing - Original draft*: Piero Poli, Josipa Majstorović, T. Dylan Mikesell.

Abstract Broadband seismometers, though designed to record ground motion generated by earthquakes, are also sensitive to a wide range of other processes occurring at the interface between the solid Earth, oceans, and atmosphere, often considered noise. In the sub-seismic band (1–24 hours), they can detect tidal signals but are limited by self-noise for weaker Earth and atmospheric processes. By applying a coherence-based network stacking technique to large seismic arrays, we identify weak, periodic gravity signals at these frequencies. Using three years of collocated vertical seismic and pressure data from USArray, we demonstrate the atmospheric origin of these oscillations. Coherence and transfer function analysis reveal strong links between pressure and seismic acceleration at atmospheric tide periods. The transfer function shows frequency dependence consistent with superconducting gravimeter observations, and its consistently negative phase indicates that pressure increases correspond to decreases in gravitational acceleration. This confirms Newtonian attraction from atmospheric mass changes as the dominant mechanism. Our results show that network stacks of broadband seismometers can detect atmospheric gravity variations as small as 10–100 nanogals, demonstrating their value for gravimetry and for observing atmospheric dynamics. This approach also provides a framework to estimate atmospheric noise in the sub-seismic range, improving the detection of solid Earth signals once such contamination is removed.

Production Editor: Andrea Llenos
Handling Editor: György Hetényi
Copy & Layout Editor: Tara Nye

Signed reviewer(s): Adam Ringler

Received: September 23, 2025
Accepted: March 6, 2026
Published: March 18, 2026

1 Introduction

Atmospheric pressure oscillates at an array of frequencies in response to periodic heating from the Sun (Lindzen and Chapman, 1969). It also responds to the gravitational pull of the Sun and the Moon, in much the same way as the solid Earth (Siebert, 1961; Lindzen and Chapman, 1969; Agnew, 2009). These continuous *tidal* oscillations of the atmosphere are primarily studied using satellite data (He et al., 2019; Forbes and Garrett, 1979), but their signature is also recorded as pressure oscillations in barometers at the Earth's surface (Crossley et al., 2013; Merriam, 1992; Warburton and Goodkind, 1977; Rosat et al., 2014; Hedlin et al., 2018).

For solid Earth geophysics, understanding these signals is fundamental, as atmospheric pressure oscillations can also be detected in gravitational acceleration (or gravity) measurements at the Earth's surface (Crossley et al., 2013; Merriam, 1992; Warburton and Goodkind, 1977; Rosat et al., 2014). Pressure dynamics influences geophysical observations through three primary mechanisms: inertia, elastic deformation of the Earth, and Newtonian attraction (Dahlen and Tromp, 1999). Among these, Newtonian attraction, caused by variations in atmospheric mass, has the strongest effect at sub-seismic periods (defined here as 1 to 24 hours). The maximum theoretical gravity-to-pressure perturbation ratio for this effect is given by Zürn and Wielandt (2007):

$$\frac{\Delta g}{\Delta P} = -4.24 \times 10^{-11} \, \frac{\mathrm{m/s^2}}{\mathrm{Pa}}. \tag{1}$$

This relationship suggests that typical pressure variations induced by atmospheric tides, on the order of tens to hundreds of Pascals (Hedlin et al., 2018; Freybourger et al., 1997), generate gravity perturbations of approximately 10^{-7} to 10^{-9} m/s^2.

Although small in amplitude, these gravity perturbations are of critical importance in solid Earth studies. They are typically observed with highly sensitive instruments, such as superconducting gravimeters, and they are often considered noise in geophysical investigations because they can mask subtle signals associated with internal geodynamic processes (Crossley et al., 2013, 1992). As a result, significant efforts have been made to model and correct for the influence of atmospheric dynamics on gravity measurements (Boy et al., 1998; Crossley et al., 2013; Hinderer et al., 2014; Merriam, 1992; Rosat et al., 2014; Warburton and Goodkind, 1977). These studies have revealed that the admittance between air pressure and gravity is both time- and frequency-dependent, and that a global atmospheric model is often required to accurately predict gravity variations due to atmospheric pressure fluctuations (Boy et al., 1998, 2002; Warburton and Goodkind, 1977).

Seismometers, which in theory should be capable of measuring gravity perturbations at sub-seismic fre-

*Corresponding author: piero.poli@unipd.it

quencies (Lambotte et al., 2006; Rosat et al., 2014), are nonetheless significantly noisier than other geophysical instruments such as superconducting gravimeters (Rosat et al., 2014). However, broadband seismic stations are far more numerous and have recorded continuous data over several decades on a global scale. This makes them an invaluable dataset for investigating signals potentially associated with geodynamic processes (Boy et al., 1998; Crossley et al., 2013; Hinderer et al., 2014; Merriam, 1992; Rosat et al., 2014; Warburton and Goodkind, 1977).

Despite this potential, relatively few studies have explored the capability of seismometers to detect gravity-related signals at sub-seismic periods (Lambotte et al., 2006; Rosat et al., 2014; Martynov et al., 2020; Freybourger et al., 1997). Some studies demonstrated that broadband seismometers can resolve gravity signals associated with the main tidal components of the solid Earth at periods up to 8 hours and with amplitudes exceeding ∼100 nanogals. Nevertheless, instrumental noise remains a major limitation, often preventing the detection of weaker signals (Lambotte et al., 2006; Rosat et al., 2014; Martynov et al., 2020; Freybourger et al., 1997).

In a recent work, Poli et al. (2025) introduced a coherence-based stacking approach using global seismic arrays to enhance the sensitivity of seismometers at sub-seismic periods. This array processing method significantly improved the signal-to-noise ratio of the data, enabling resolution of acceleration signals on the order of a few nanogals, comparable to both theoretical and observed tidal amplitudes, and well beyond the traditional resolution limits of single seismometers. The technique enabled observation of spectral peaks at integer fractions of one day, which were interpreted to be driven by atmospheric tides. Crucially, Poli et al. (2025) showed that by treating seismic networks as coherent sensor arrays, it becomes possible to monitor acceleration variations with nanogal-level precision, offering a new pathway to study both internal Earth processes and global atmospheric dynamics using broadband seismic array data.

The objective of the current study is to establish a quantitative link between persistent harmonic signals recorded by seismometers at sub-seismic periods and pressure variations due to atmospheric tides. To this end, we extend the methodology of Poli et al. (2025) to a network of collocated barometers and broadband seismic sensors across the eastern United States (Figure 1), with a particular focus on the data processing pipeline required to detect these weak harmonic signals. We then quantify how the atmospheric tides influence surface pressure, and how these, in turn, generate gravitational acceleration variations observable in seismic data. For this, it is essential to use the long time series of barometric data recorded at the exact same location as the seismic station.

Our approach builds on techniques developed for superconducting gravimeters and adapts them to arrays of barometers and broadband seismometers. We compute the coherence and transfer function between pressure and seismic gravity signals using collocated instrument data. The results provide direct observational evidence for the atmospheric origin of sub-seismic harmonic signals in seismic records. Furthermore, we empirically constrain the frequency-dependent admittance between pressure and local gravitational acceleration, establishing a foundation for correcting atmospheric effects in seismic data and potentially enhancing the detection of subtle geodynamic signals (Crossley et al., 1992). This work also demonstrates that broadband seismic networks can serve as a valuable complement to gravimeters, offering new opportunities to study gravity changes related to both surface and deep Earth processes.

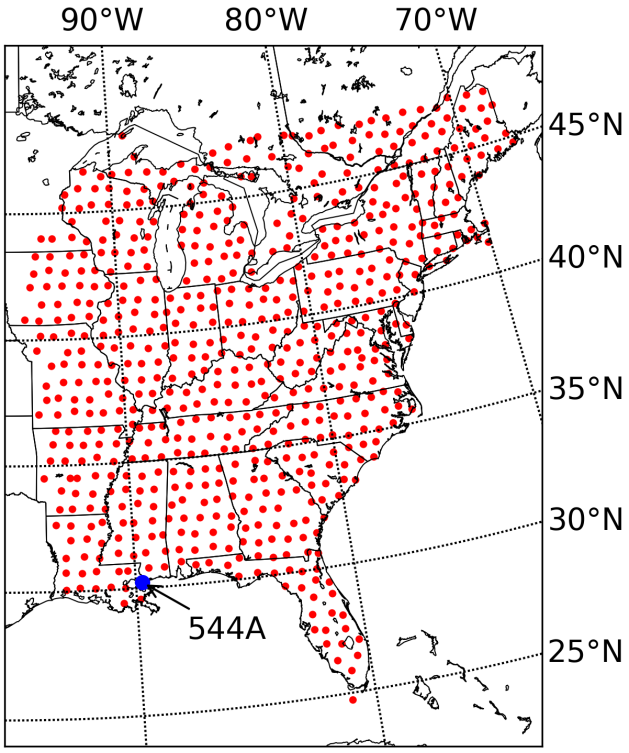

Figure 1 Map of the collocated seismic and barometric pressure stations (red dots) used in this study.

2 Pressure and acceleration data

We used data from the USArray recorded during the period January 2012 to December 2014 (Figure 1). During this time, 718 broadband seismic stations were located together with a SETRA 278 barometer (channel LDO), whose response is flat in the sub-seismic frequency range and samples barometric pressure at 1 Hz (Tytell et al., 2016). The seismological data were recorded using broadband and very broadband seismometers (Streckeisen STS-2 , Guralp CMG-3T, Teledyne-Geotech KS54000). We analyzed the vertical component seismic data (channel VHZ) sampled at 0.1 Hz . We downloaded the seismic and pressure data over the entire three-year analysis period in segments of 10 days with a 5-day overlap.

The downloaded raw data were preprocessed to obtain acceleration in m/s^2 (from seismometers) and pressure in Pascal (from barometers). Specifically, we

removed the instrument response from the seismological data using water-level deconvolution following Beyreuther et al. (2010). Before performing deconvolution, the mean of the data was removed, and bandpass filtering was applied with cutoff frequencies of: $1/f_1 = 5$ days, $1/f_2 = 4$ days, $1/f_3 = 3000$ s, $1/f_4 = 2000$ s. We tested various values of the water level parameter in a range from 0 to 200. For each water level value, the amplitude of the output signal was compared to the expected acceleration of solid Earth tides at 1 and 2 cycles per day (cpd). We found that for water level values above 60, the seismometer amplitudes matched the predicted accelerations for daily and half-daily solid tides. Based on this, we set a final water level value of 80 for all seismic data. For pressure data, the same parameters were used for deconvolution. In the final step, we resampled the pressure (channel LDO) and acceleration time series from 0.1 Hz and 1 Hz, respectively, to 0.001 Hz, and synchronized the data segments by interpolating both time series onto a common time vector. We retained only the 10-day segments without gaps or zeros to avoid additional corrections to these data, which represent up to 70% of the initial dataset.

3 Array coherence for pressure and acceleration data

To resolve small gravity signals with seismometers in sub-seismic periods, we applied the array processing of Poli et al. (2025) and Takano and Poli (2024) to the USArray data. In the Fourier domain, we calculated the coherence between the data (S) recorded at each pair of stations (i, j) for the VHZ and LDO channels independently (e.g., Figure 2a), over an ensemble of M time windows (Bendat and Piersol, 2010; Takano and Poli, 2024):

$$C_{ij}^{T}(f) = \frac{1}{M} \frac{\sum_{t=1}^{M} S_{i,t}(f) \cdot S_{j,t}^{*}(f)}{\sum_{t=1}^{M} \sqrt{S_{i,t}^{2}(f) \cdot S_{j,t}^{2}(f)}}. \quad (2)$$

Each time window T is 10 days, and the time series data were tapered using a Hanning window before computing the Fourier transform. The total number of windows M was variable, depending on the available LDO or VHZ data segments. However, we ensured that $M > 20$ (200 days of data) for a reliable estimate of coherence (Equation 2).

We computed two different kinds of coherence to determine if further processing had an influence on the results. We used raw signals from deconvolution without additional processing (C_r), and we also calculated another set of coherence after spectral whitening (C_w), which consisted of normalizing the amplitude of each signal in the frequency domain $|S(f)|$ to 1, preserving only the phase for the computation of coherence. The latter has been shown to enhance the resolution of weak but persistent monochromatic signals (Takano and Poli, 2024). We define the network average coherence from N stations (Figure 2b–2i) as in Takano and Poli (2024):

$$\tilde{C}(f) = \frac{2}{N(N-1)} \sum_{i=1}^{N} \sum_{j=i+1}^{N} |C_{ij}^{T}(f)|, \quad (3)$$

for the two different sets of coherence (C_r and C_w).

The stack of seismological data (Figure 2b–2e) closely resembles the results of the global analysis by Poli et al. (2025), showing strong signals near 1, 2, and 3 cpd, which correspond to the dominant lunisolar tidal harmonics (Agnew, 2009), as well as peaks at integer fractions of one day, observable up to 11 cpd. Above 3 cpd, a notable difference emerges between the stack of raw data (Figure 2e) and that of whitened data (Figure 2c). The whitened data more clearly resolve small-amplitude peaks and exhibit a flatter background coherence spectrum. In the whitening process, amplitude information is removed while phase is preserved, such that Equation 3 simplifies to a phase difference between signals. This enhances the detection of features resulting from sustained excitation over time, as recently demonstrated in studies of volcanic tremor and persistent monochromatic signals (Barajas et al., 2024; Takano and Poli, 2024). In other words, whitening facilitates the resolution of even very small signals, provided their phase remains stable over time. Stacking further reinforces these signals while suppressing the influence of transient amplitude variations. The effect of different data processing, however, does not significantly alter the coherence estimated for pressure data (Figure 2f–2i), suggesting a limited impact of transients in the pressure dataset. The stack of pressure data (Figure 2f–2i) reveals a similar structure to that observed in seismic data, with coherence peaks that are mostly located at integer fractions of one day. This behaviour is expected, as marginal contribution from solid tides is expected in the pressure data, or frequencies above 3 cpd. The peaks occur at frequencies related to the solar day and can be attributed to atmospheric tides (Lindzen and Chapman, 1969).

The striking similarity in coherence between the seismic and pressure data, particularly in the peak frequencies above 3 cpd (Figure 3a), supports the hypothesis of Poli et al. (2025) that the observed seismic peaks have an atmospheric origin. However, the relative amplitudes of the coherence peaks differ between the two datasets, and no strong correlation is apparent (Figure 3b-c). This suggests a frequency-dependent relationship between the seismological gravity records and surface pressure. To further investigate this, we explore the coherence and transfer function between the two datasets in the following section.

4 Coherence and transfer function between pressure and acceleration

To better understand the relationship between pressure and acceleration signals observed at sub-seismic frequencies, we estimate the coherence (Equation 2) and the pressure-normalized transfer function (TF) between the LDO (P) and VHZ (S) channels at each station i, using a window length T.

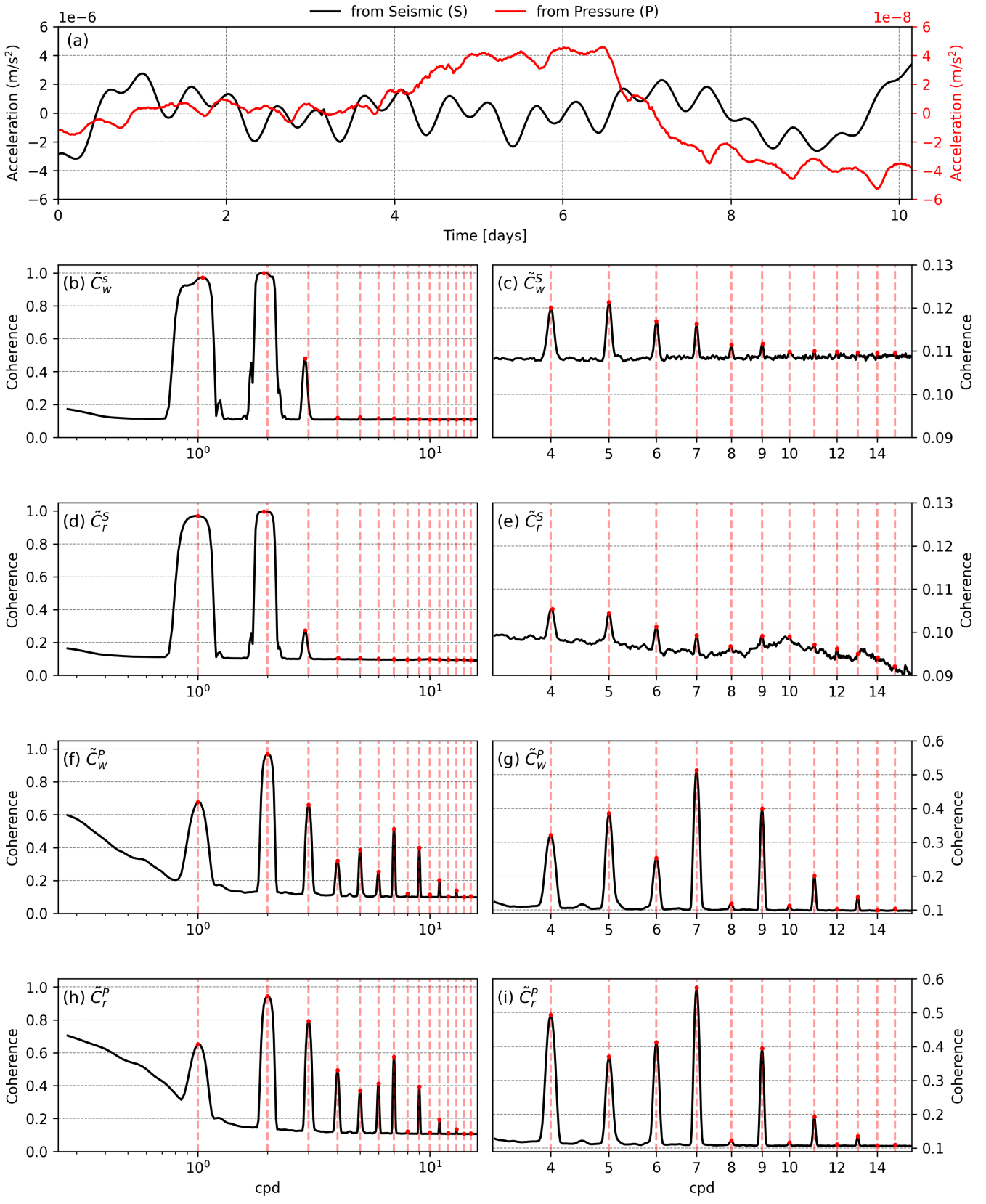

Figure 2 (a) Example times series of the preprocessed seismic and pressure data converted to units of acceleration using Equation 1 from station 544A (Figure 1). (b,c) Array averaged coherence of whitened seismic data $\tilde{C}_w^S$; (d,e) non-whitened seismic data $\tilde{C}_r^S$; (f,g) whitened pressure data $\tilde{C}_w^P$; (h,i) non-whitened pressure data $\tilde{C}_r^P$. Vertical dashed lines are the integer fractions of each day, while red dots (b-i) indicate the largest local amplitude peaks nearest (i.e., $\pm$ 0.75 cpd) to the integer fraction of one day.

The TF provides an estimate of the admittance between pressure and acceleration and, unlike the coherence (Equation 2), offers physical insight through its units. In particular, it allows us to quantify how much

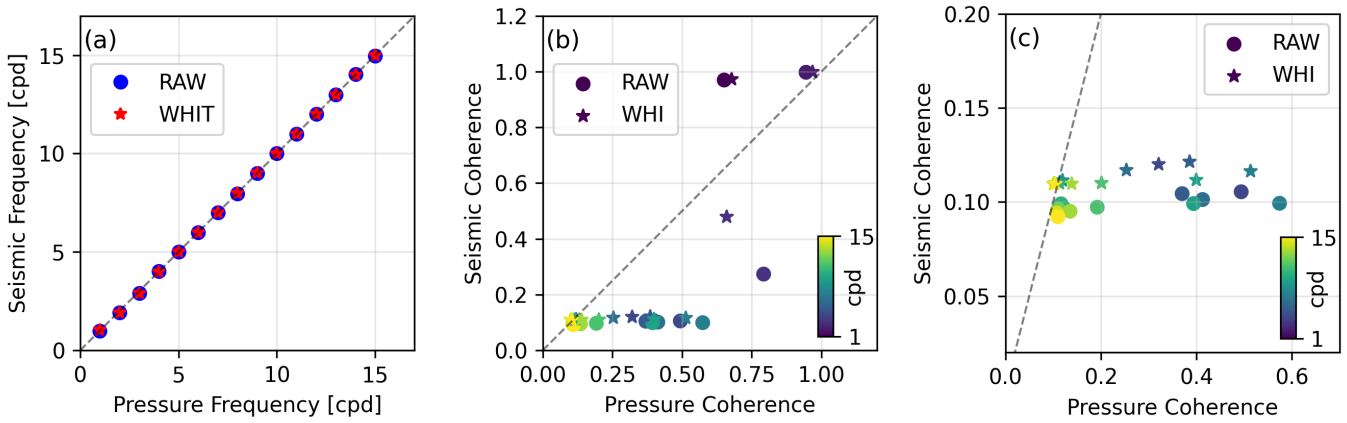

Figure 3 (a) Comparison of the peak frequencies for pressure and seismic data. (b) Comparison of the peak coherence values. c) Zoom around low peak coherence values. Dashed black line in all plots is the one-to-one line.

atmospheric pressure is transferred into ground acceleration. The transfer function is defined as:

$$TF_i^T(f) = \frac{1}{M}\frac{\sum_{t=1}^{M} S_i(f)\cdot P_i^*(f)}{\sum_{t=1}^{M} P_i^2(f)}, \quad (4)$$

(Boy et al., 2002; Rosat et al., 2014; Warburton and Goodkind, 1977). In the following analysis we set the window length $T = 10$ days.

The overall structure of the LDO–VHZ coherence (Figure 4a) reveals prominent peaks at integer multiples of one day, indicating a strong correlation between vertical ground acceleration (VHZ) and surface pressure (LDO). This observation supports the hypothesis that atmospheric tides can be resolved in seismic acceleration records. In other words, while atmospheric tides manifest as pressure variations, they also influence acceleration measurements through gravitational effects. Furthermore, we observe a nearly linear increase in coherence across the analyzed frequency band, from lower to higher frequencies, which is consistent with previous studies based on collocated gravimeters and barometers (e.g., Merriam, 1992; Rosat et al., 2014), linked to the frequency dependent contribution of Newtonian attraction, free air and inertial effects (Zürn and Wielandt, 2007).

To further investigate the observed correspondence between acceleration and pressure, and to elucidate the physical mechanism driving the recorded acceleration in the seismometers, we evaluate both the magnitude and the sign of the transfer function between the LDO and VHZ data.

$$|TF^{net}(f)| = 10^{\frac{1}{N}\sum_{i=1}^{N} log(|TF_i^T(f)|)}, \quad (5)$$

$$cos(\Phi^{net}(f)) = atan\left(\frac{1}{N}\sum_{i=1}^{N}\cos(\theta_i), \frac{1}{N}\sum_{i=1}^{N}\sin(\theta_i)\right), \quad (6)$$

where the angles θ are estimated from the complex values of TF.

The magnitude of TF (Figure 4b) shows a clear frequency dependence, with an average value of 1.69×10^{-10} m/s^2 Pa^{-1} observed from 3.2 to 16 cpd; this range excludes periods also influenced by the solid Earth tides (< 3.2 cpd) and highlights the atmosphere-driven component of the signal. Distinct drops in magnitude are observed at integer fractions of 1 day, consistent with previous studies on superconducting gravimeters (Hinderer et al., 2014; Warburton and Goodkind, 1977; Rosat et al., 2014). The average magnitude of the admittance is 4 times larger than the theoretical expectation from Newtonian attraction (Equation 1).

The average admittance is within a factor of 2 of previous estimates obtained from very-broadband seismometers (Lambotte et al., 2006; Rosat et al., 2014). Importantly, unlike these earlier studies, our measurements are able to resolve peaks at integer fractions of a day for frequencies above approximately 3 cpd, revealing details that were previously inaccessible.

The difference of a factor of 4 between admittance estimated from seismological and gravity data can be attributed to higher self-noise levels in seismometers at sub-seismic frequencies, to possible amplification of the gravity signal, or to attenuation of pressure during the correction of instrument response. These potential causes should be explored in future studies. A similar deviation between external forcing and seismometer response for tidal signals has been previously reported (Davis and Berger, 2007). Despite this small amplitude discrepancy, the overall frequency dependence is similar to the admittance estimated using superconducting gravimeters (Hinderer et al., 2014; Warburton and Goodkind, 1977; Rosat et al., 2014), whereby admittance decreases at integer fractions of one day because atmospheric tides significantly influence atmospheric dynamics (Lindzen and Chapman, 1969). Furthermore, a reduction in admittance is observed for frequencies exceeding 9 cpd (Figure 4b) (Hinderer et al., 2014; Warburton and Goodkind, 1977; Rosat et al., 2014).

The sign of the transfer function (Equation 6) is negative, with values close to -1 for the full spectral range analyzed (Figure 4c). This indicates that an increase in pressure induces a decrease in acceleration and vice versa. At sub-seismic frequencies, Newtonian attraction should dominate the measurement compared

to elastic displacement or inertia (Zürn and Wielandt, 2007; Dahlen and Tromp, 1999). For atmospheric density oscillations around an average value, at the moment of maximum positive density (positive pressure), we expect an upward motion of the seismometer mass and the opposite behavior (downward motion of the mass) for negative pressure, reflecting negative density changes. Thus, the expected effect of Newtonian attraction would result in an admittance value with a negative sign (Equation 1). Our results agree with this negative admittance behavior, regardless of the applied processing (raw or whitened, Figure 4c). To demonstrate that the negative value does not arise from averaging random phases, we replace the angles estimated from the transfer function at each station with random values ranging from $-\pi$ to π. Averaging these signals as in Equation 6 results in randomly distributed signs of TF with frequency (Figure 4c). The results in Figure 4 clearly reflect the theoretical expectations for Newtonian attraction (Zürn and Wielandt, 2007) and experimental estimates of gravity behavior at sub-tidal periods, supporting the hypothesis (Poli et al., 2025) that the observed coherent peaks in array stacks of acceleration measurements from seismometers are sensitive to pressure variations which correlate with periods associated with the atmospheric tides.

Our results generally agree with previous studies, but they are not without caveats. Unlike earlier work (e.g., Boy et al., 1998; Crossley et al., 2013; Hinderer et al., 2014; Merriam, 1992; Rosat et al., 2014; Warburton and Goodkind, 1977), which typically estimate a single transfer function between a gravimeter and a collocated barometer, it is important to emphasize that we do not rely on data from a single instrument. As a result, both the pressure-acceleration coherence and the pressure-normalized transfer function represent averages over time and space. Consequently, based on the results shown in Figure 4, we cannot resolve spatial or temporal variations in admittance across the different datasets (Boy et al., 1998, 2002; Warburton and Goodkind, 1977). In other words, our estimates may be influenced by the spatio-temporal evolution of admittance (Hinderer et al., 2014), beyond the observed frequency dependence (Figure 4). However, a detailed local spatio-temporal analysis of admittance using seismometers is limited by their higher noise levels compared to instruments such as superconducting gravimeters (Hinderer et al., 2014). Therefore, we must rely on stacking approaches to test whether, as observed in previous studies (Hinderer et al., 2014), we can obtain an admittance that varies in space and time.

To explore the temporal and spatial variability of the admittance, we focus on the 7 cpd peak, which is the largest peak observed in both the seismic and pressure data (Figure 2). For this purpose, we average the transfer functions over 3-month intervals with a 2-month overlap. The results in Figure 5a reveal an admittance systematically larger than that estimated using Equation 1, with a temporal variability within a factor of 6.

In addition, we perform a spatial stacking, defining a transfer function (Equation 5) as the average of all transfer functions for stations located within 2° of each station. The map in Figure 5b at 7 cpd illustrates significant spatial variability, with admittance varying within a factor of 4.

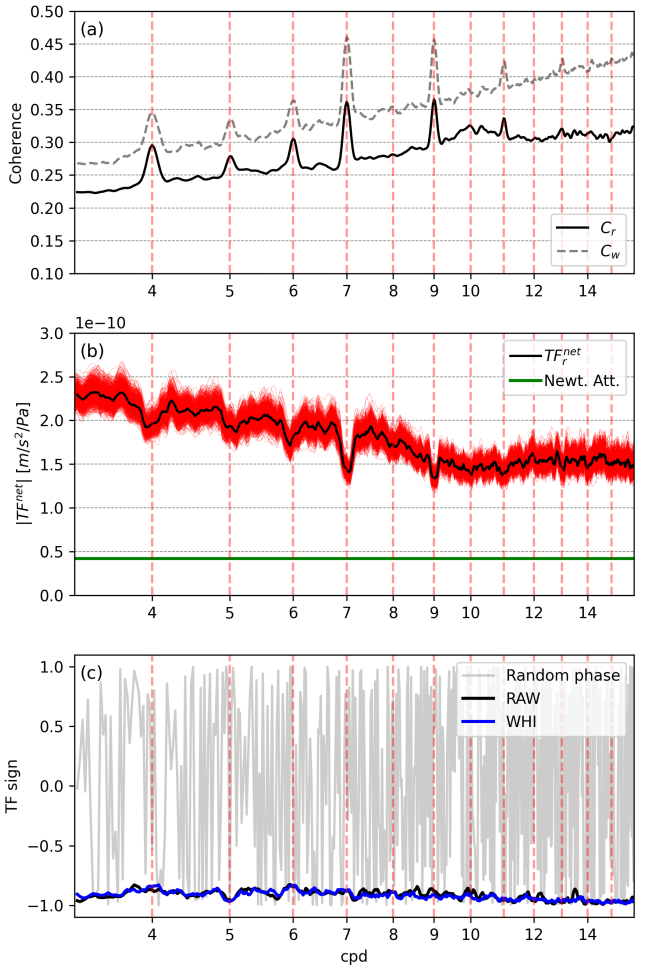

Figure 4 (a) Coherence between raw and whitened LDO (P) and VHZ (S) data. (b) Mean transfer function magnitude (TF^{net}) across the network (Equation 5) of raw data (black) together with 1000 bootstrapped versions of the mean TF from 500 randomly sampled raw TF (red). The admittance from Newtonian attraction (Equation 1) is also reported in green. (c) Sign of the transfer function (Equation 6) for raw and whitened data. The gray line is the sign obtained from averaging random angles.

It is important to note that the choice of temporal and spatial stacking windows is somewhat arbitrary and was determined empirically to ensure that coherent peaks and statistically meaningful transfer functions, supported by sufficient data during stacking, are observed at the target frequency of 7 cpd. The robustness of these results will be the subject of future studies.

We emphasize again that the results presented in Figure 5 are not directly comparable with the estimates reported in Hinderer et al. (2014), as our analysis provides an average picture. Nevertheless, even in this averaged form, the results reveal an admittance pattern that cannot be obtained with current gravimetric studies. Furthermore, these results indicate that, despite our overall stacking procedure being useful to constrain atmospheric effects in seismometers at previously unexplored frequencies, a precise correction of atmospheric

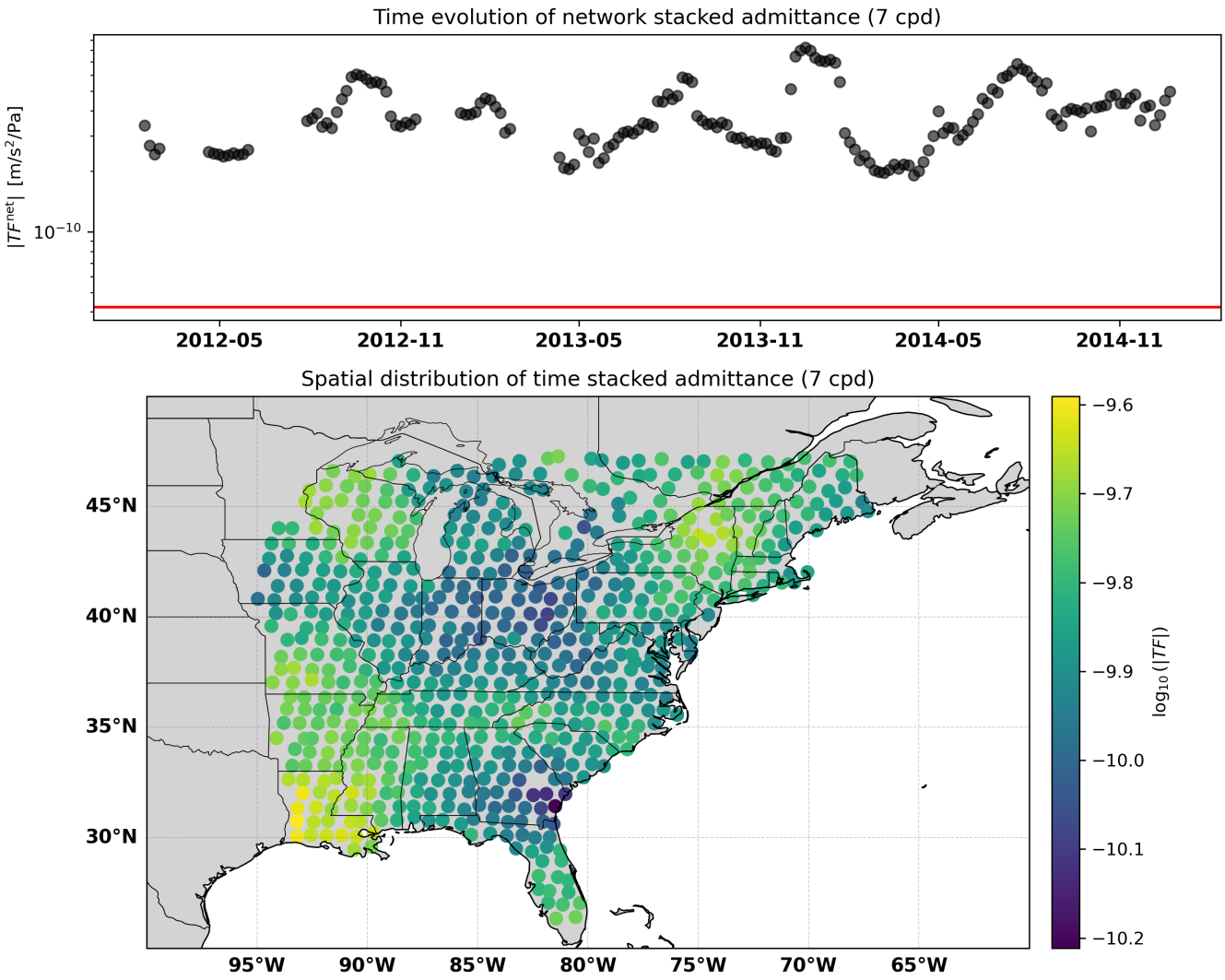

Figure 5 (a) Temporal evolution of network-stacked admittance at 7 cpd. The red line represents the admittance from Equation 1. (b) Spatial variation of admittance at 7 cpd with a network stack radius of 2° from each station.

effects for geodynamical purposes (Rosat et al., 2003; Hinderer et al., 2014) must account for the spatial and temporal evolution of the admittance. The development of an appropriate correction scheme based on stacked average admittance is the subject of ongoing and future research.

5 Discussion and Conclusions

We report an increase in coherence between barometric and seismological observations at integer fractions of one day (Figure 4a), highlighting a causal relationship between the two signals and supporting the atmospheric origin of the seismological observations due to atmospheric tides (Poli et al., 2025). This observation, unlike previous studies based on single seismometers and limited time windows (Rosat et al., 2014), indicates a direct relationship between atmospheric dynamics and local gravitational acceleration measured by seismometers, which can only be revealed through stacking. The network-averaged transfer function is used to estimate the frequency-dependent admittance, including the sign of the response between pressure and acceleration. The average admittance values and their signs are consistent with theoretical expectations based on a Newtonian attraction model (Zürn and Wielandt, 2007), and they agree with previous estimates derived from superconducting gravimeters (Hinderer et al., 2014; Warburton and Goodkind, 1977; Rosat et al., 2014).

Although the value and phase of the transfer function indicate the physical origin of the acceleration peaks at sub-seismic frequencies, applying this transfer function to correct acceleration data is not straightforward. As we average over time and space (Equation 5), our estimate may not capture potential spatio-temporal variations in the admittance, which have been documented in previous studies (Hinderer et al., 2014). Nevertheless, the estimation of the transfer function obtained through random resampling of Equation 5 reveals a relatively stable behaviour, with values typically confined within a factor of two or less. The space and time variability of admittance, which we documented in Figure 5, remains the main challenge for correction of atmospheric effects in seismological data, and it will be subject of future studies.

Another important result of our analysis concerns

data processing choices and highlights the benefits of whitening. Although the whitening technique entirely discards amplitude information, it effectively reduces the influence of transient signals (e.g., long-period noise variations, spikes, glitches), while enhancing temporally stable (i.e., stationary) signals such as solid Earth and atmospheric tides (Figure 2). Thus, this approach may also prove valuable in increasing the signal-to-noise ratio when stacking alternative datasets in the search for geodynamical signals (Cummins et al., 1991; Rosat et al., 2003).

Overall, this study illustrates that stacking acceleration data recorded by broadband seismometers in the sub-seismic frequency band enhances the observation of subtle gravity signals. It shows that these signals are dominated by atmospheric tides at integer fractions of one day for frequencies above ∼3 cpd, which induce gravity perturbations of the order of ∼10 to 100 nanogals (Equation 1). With the resolution achieved through stacking, the broadband seismic network can serve as a valuable new tool for integrating gravity studies aimed at detecting geodynamic signals (e.g., Crossley et al., 1992), particularly through the development of strategies to mitigate atmospheric influences on seismometers at sub-seismic frequencies. Finally, this study demonstrates that, in the absence of barometric or gravimetric data, seismometers can be used to track long-period signals associated with atmospheric dynamics (Lindzen and Chapman, 1969; He et al., 2019, 2024; Hedlin et al., 2018). This is particularly advantageous because networks of modern seismometers provide near-global coverage and long-term data continuity, making them one of the most reliable large-scale observational systems in existence on Earth.

Acknowledgements

TDM acknowledges that the preparation of this article was partially supported by basic funding to NGI from the Research Council of Norway. We would like to thank Adam Ringler and the two anonymous reviewers for their insightful comments, which helped to improve the manuscript.

Data and code availability

Barometric and seismological data used in this study are from USArray (IRIS Transportable Array, 2003), and can be accessed from the NSF SAGE data archive operated by EarthScope Consortium (NSF award 1724509). All analyses were performed using Python (Van Rossum and Drake, 2009) with the `SciPy` (Virtanen et al., 2020), `NumPy` (Harris et al., 2020), and `ObsPy` (Beyreuther et al., 2010) libraries.

Competing interests

The authors have no competing interests.

References

Agnew, D. C. Earth Tides. In Schubert, G., editor, *Treatise on Geophysics*, volume 3, pages 163–195. Elsevier, 2009. doi: 10.1016/B978-044452748-6.00060-3.

Barajas, A., Shapiro, N., and Prieto, G. Differential phase analysis for volcanic tremor detection and source location. In *EGU General Assembly 2024*, pages EGU24–16604, Vienna, Austria, 2024. doi: 10.5194/egusphere-egu24-16604.

Bendat, J. S. and Piersol, A. G. *Random Data: Analysis and Measurement Procedures*. Wiley, Jan. 2010. doi: 10.1002/9781118032428.

Beyreuther, M., Barsch, R., Krischer, L., Megies, T., Behr, Y., and Wassermann, J. ObsPy: A Python toolbox for seismology. *Seismological Research Letters*, 81(3):530–533, 2010. doi: 10.1785/gssrl.81.3.530.

Boy, J.-P., Hinderer, J., and Gegout, P. Global atmospheric loading and gravity. *Physics of the Earth and Planetary Interiors*, 109(3-4):161–177, 1998.

Boy, J.-P., Gegout, P., and Hinderer, J. Reduction of surface gravity data from global atmospheric pressure loading. *Geophysical Journal International*, 149(2):534–545, May 2002. doi: 10.1046/j.1365-246x.2002.01667.x.

Crossley, D., Hinderer, J., and Riccardi, U. The measurement of surface gravity. *Reports on Progress in Physics*, 76(4):046101, Mar. 2013. doi: 10.1088/0034-4885/76/4/046101.

Crossley, D. J., Rochester, M. G., and Peng, Z. R. Slichter modes and Love numbers. *Geophysical Research Letters*, 19(16):1679–1682, Aug. 1992. doi: 10.1029/92gl01574.

Cummins, P., Wahr, J. M., Agnew, D. C., and Tamura, Y. Constraining core undertones using stacked IDA gravity records. *Geophysical Journal International*, 106(1):189–198, 1991.

Dahlen, F. A. and Tromp, J. *Theoretical Global Seismology*. Princeton University Press, Dec. 1999. doi: 10.1515/9780691216157.

Davis, P. and Berger, J. Calibration of the Global Seismographic Network Using Tides. *Seismological Research Letters*, 78(4):454–459, July 2007. doi: 10.1785/gssrl.78.4.454.

Forbes, J. M. and Garrett, H. B. Theoretical studies of atmospheric tides. *Reviews of Geophysics*, 17(8):1951–1981, Nov. 1979. doi: 10.1029/rg017i008p01951.

Freybourger, M., Hinderer, J., and Trampert, J. Comparative study of superconducting gravimeters and broadband seismometers STS-1/Z in seismic and subseismic frequency bands. *Physics of the Earth and Planetary Interiors*, 101(3–4):203–217, May 1997. doi: 10.1016/s0031-9201(97)00003-4.

Harris, C. R., Millman, K. J., van der Walt, S. J., Gommers, R., Virtanen, P., Cournapeau, D., Wieser, E., Taylor, J., Berg, S., Smith, N. J., Kern, R., Picus, M., Hoyer, S., van Kerkwijk, M. H., Brett, M., Haldane, A., del Río, J. F., Wiebe, M., Peterson, P., Gérard-Marchant, P., Sheppard, K., Reddy, T., Weckesser, W., Abbasi, H., Gohlke, C., and Oliphant, T. E. Array programming with NumPy. *Nature*, 585(7825):357–362, Sept. 2020. doi: 10.1038/s41586-020-2649-2.

He, M., Forbes, J. M., Chau, J. L., et al. High-order solar migrating tides quench at SSW onsets. ESS Open Archive, Dec. 2019. doi: 10.1002/essoar.10501510.1.

He, M., Forbes, J. M., Jacobi, C., Li, G., Liu, L., Stober, G., and Wang, C. Observational verification of high-order solar tidal harmonics in the Earth's atmosphere. *Geophysical Research Letters*, 51(8), Apr. 2024. doi: 10.1029/2024gl108439.

Hedlin, M. A. H., de Groot-Hedlin, C. D., Forbes, J. M., and Drob, D. P. Solar Terminator Waves in Surface Pressure Observations. *Geophysical Research Letters*, 45(10):5213–5219, May 2018. doi:

10.1029/2018gl078528.

Hinderer, J., Hector, B., Boy, J.-P., Riccardi, U., Rosat, S., Calvo, M., and Littel, F. A search for atmospheric effects on gravity at different time and space scales. *Journal of Geodynamics*, 80:50–57, Oct. 2014. doi: 10.1016/j.jog.2014.02.001.

IRIS Transportable Array. USArray Transportable Array, 2003. doi: 10.7914/SN/TA.

Lambotte, S., Rivera, L., and Hinderer, J. Vertical and horizontal seismometric observations of tides. *Journal of Geodynamics*, 41(1–3):39–58, Jan. 2006. doi: 10.1016/j.jog.2005.08.021.

Lindzen, R. S. and Chapman, S. Atmospheric tides. *Space science reviews*, 10:3–188, 1969.

Martynov, V. G., Astiz, L., Kilb, D., and Vernon, F. L. The M_2 Tidal Tilt Results from USArray Seismic Data from the Western United States. *Bulletin of the Seismological Society of America*, 110(6): 3196–3210, June 2020. doi: 10.1785/0120190314.

Merriam, J. B. Atmospheric pressure and gravity. *Geophysical Journal International*, 109(3):488–500, June 1992. doi: 10.1111/j.1365-246x.1992.tb00112.x.

Poli, P., Majstorović, J., Mikesell, T. D., and Lott, M. Toward Unraveling Sub-Seismic Frequency Signals Using Stacked Global Broadband Seismological Data. *Geophysical Research Letters*, 52(6), Mar. 2025. doi: 10.1029/2024gl114211.

Rosat, S., Hinderer, J., Crossley, D., and Rivera, L. The search for the Slichter mode: comparison of noise levels of superconducting gravimeters and investigation of a stacking method. *Physics of the Earth and Planetary Interiors*, 140(1–3):183–202, Nov. 2003. doi: 10.1016/j.pepi.2003.07.010.

Rosat, S., Calvo, M., Hinderer, J., Riccardi, U., Arnoso, J., and Zürn, W. Comparison of the performances of different spring and superconducting gravimeters and STS-2 seismometer at the Gravimetric Observatory of Strasbourg, France. *Studia Geophysica et Geodaetica*, 59(1):58–82, Nov. 2014. doi: 10.1007/s11200-014-0830-5.

Siebert, M. Atmospheric Tides. In Landsberg, H. and Mieghem, J. V., editors, *Advances in Geophysics*, volume 7 of *Advances in Geophysics*, pages 105–187. Elsevier, 1961. doi: 10.1016/S0065-2687(08)60362-3.

Takano, T. and Poli, P. Coherence-based characterization of a long-period monochromatic seismic signal. Authorea, Oct. 2024. doi: 10.22541/au.173030428.85120620/v1.

Tytell, J., Vernon, F., Hedlin, M., de Groot Hedlin, C., Reyes, J., Busby, B., Hafner, K., and Eakins, J. The USArray Transportable Array as a Platform for Weather Observation and Research. *Bulletin of the American Meteorological Society*, 97(4):603–619, Apr. 2016. doi: 10.1175/bams-d-14-00204.1.

Van Rossum, G. and Drake, F. L. *Python 3 Reference Manual*. CreateSpace, Scotts Valley, CA, 2009.

Virtanen, P., Gommers, R., Oliphant, T. E., Haberland, M., Reddy, T., Cournapeau, D., Burovski, E., Peterson, P., Weckesser, W., Bright, J., van der Walt, S. J., Brett, M., Wilson, J., Millman, K. J., Mayorov, N., Nelson, A. R. J., Jones, E., Kern, R., Larson, E., Carey, C. J., Polat, İ., Feng, Y., Moore, E. W., VanderPlas, J., Laxalde, D., Perktold, J., Cimrman, R., Henriksen, I., Quintero, E. A., Harris, C. R., Archibald, A. M., Ribeiro, A. H., Pedregosa, F., van Mulbregt, P., and SciPy 1.0 Contributors. SciPy 1.0: fundamental algorithms for scientific computing in Python. *Nature Methods*, 17(3):261–272, Feb. 2020. doi: 10.1038/s41592-019-0686-2.

Warburton, R. J. and Goodkind, J. M. The influence of barometric-pressure variations on gravity. *Geophysical Journal International*, 48(3):281–292, Mar. 1977. doi: 10.1111/j.1365-246x.1977.tb03672.x.

Zürn, W. and Wielandt, E. On the minimum of vertical seismic noise near 3 mHz. *Geophysical Journal International*, 168(2):647–658, Feb. 2007. doi: 10.1111/j.1365-246x.2006.03189.x.